

# Deterministic control of photonic de Broglie waves using coherence optics: Coherence de Broglie waves

Byoung S. Ham

Center for Photon Information Processing, School of Electrical Engineering and Computer Science, Gwangju  
Institute of Science and Technology  
123 Chumdangwagi-ro, Buk-gu, Gwangju 61005, S. Korea  
(Submitted on January 28, 2020)  
bham@gist.ac.kr

In quantum mechanics, photonic de Broglie waves have been understood as a unique property of quantum mechanics satisfying the complementarity between particle and wave natures of light, where the photonic de Broglie wavelength is inversely proportional to the number of entangled photons acting on a beam splitter. Very recently, the heart of nonclassical feature of photon bunching on a beam splitter was newly interpreted using pure wave nature of coherence optics [arXiv:1911.07174v2], paving a road to unconditionally secured classical key distribution [arXiv:1807.04233v3]. Here, Mach-Zehnder interferometer-based deterministic photonic de Broglie waves are studied in a coherence regime for both fundamental physics and potential applications of coherence-quantum metrology.

The nonclassical feature of anticorrelation on a beam splitter (BS), the so-called Hong-Oh-Mandel dip or photon bunching, has been the heart of quantum mechanics in terms of superposition and entanglement, where it cannot be achieved by classical means<sup>1-5</sup>. Unlike most anticorrelation studies based on statistical nature of light, a deterministic solution has been recently found in a coherence manner for a particular phase relation between two input fields impinging on a BS<sup>6</sup>. Owing to coherence optics with a phase control, the BS-based anticorrelation can be achieved in a simple Mach-Zehnder interferometer (MZI) deterministically controlling the relative phase in MZI<sup>6</sup>. One of the first applications of the MZI-based anticorrelation is the unconditionally secured classical key distribution<sup>7</sup>. Although the physics of the unconditionally secured classical key distribution is based on quantum superposition, i.e., indistinguishability in the MZI paths<sup>7</sup>, the key carrier is not a quantum but a coherent light compatible with current fiber-optic communications networks. As debated for several decades, a fundamental question about quantum nature of light is still an on-going important subject in quantum optics community<sup>8-10</sup>.

Here in this paper, a fundamental question of “what is the quantum nature of light? or “what is the origin of nonclassicality?” is asked and answered in terms of photonic de Broglie waves (PBW) in a pure coherence regime based on the wave nature of light. Due to the quantum property of linear optics such as a BS, however, the nonclassical light is also included to the present scope. Thus, the present paper is for general conceptual understanding in fundamental quantum physics as well as for potential applications of coherence-quantum metrology to overcome the statistical quantum limitations such as an extremely low rate at the higher-order entangled photon-pair generation.

The photonic de Broglie wavelength  $\lambda_B$  has been a key feature in quantum mechanics of wave-particle duality or complementarity for quantum nature of light, where classical physics has been completely blocked off<sup>11-14</sup>. The PBW has been mostly demonstrated using entangled photon pairs generated from spontaneous parametric down conversion (SPDC) process, where  $\lambda_B = \lambda_0/N$ , and  $\lambda_0$  (N) is the initial wavelength (number of entangled photons in such as a NOON state) of light<sup>11-14</sup>. For example, a single-photon entangled pair on a beam splitter results in PBW at  $\lambda_B = \lambda_0/2$ . So does  $\lambda_B = \lambda_0/4$  for a two-photon entangled pair. Due to experimental difficulties of obtaining higher-order entangled photon pairs, however, the application of quantum PBW has been severely limited so far, whose latest record is  $\lambda_B = \lambda_0/18$  with  $N=18$ <sup>14</sup>. By the same reason, quantum metrology such as quantum lithography and quantum sensing has also been limited to practical applications<sup>15-17</sup>. Most of all, there is no deterministic entangled photon pair generator. In the present paper, a deterministic control of PBW using the coherence-optics-based anticorrelation<sup>6</sup> is presented for both

fundamental physics and its potential applications of coherence-quantum metrology, where the order  $N$  in  $\lambda_B$  is potentially unlimited and on demand. The deterministic control of PBW should give a great benefit to quantum metrology beyond the standard quantum limit. The deterministic controllability of the higher-order PBW brings a breakthrough in practical limitations of the entangled photon-based conventional quantum metrology<sup>15-17</sup>. Most of all, understanding of the quantum nature of light in PBW is the most important result.

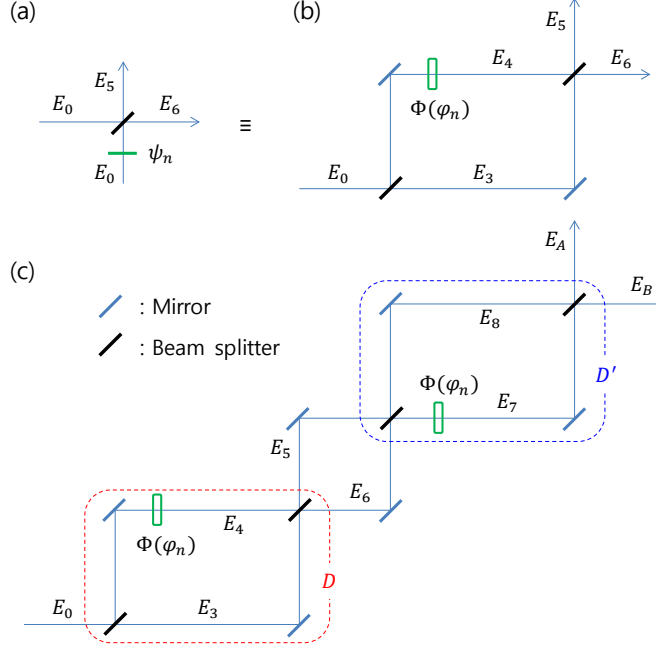


Fig. 1. A coherence scheme of anticorrelation compatible to an entangled photon state. (a) A BS-based anticorrelation scheme for photon bunching. (b) An equivalent scheme of (a) for coherence optics. (c) A basic unit of coherence PBW. The input field  $E_0$  is coherent light.  $D$  or  $D'$  indicates a MZI building block composed of beam splitters and a phase shifter. The coupled matrix of  $[D'] [D]$  represents a coherence PBW scheme equivalent to quantum PBW with  $N=4$ .

Figure 1 shows a basic building block of the present scheme for the deterministic control of PBW via coherence optics-based anticorrelation. Figure 1(a) shows an deterministic scheme of anticorrelation with a phase shifter  $\psi_n$  for photon bunching or a HOM dip on a BS<sup>6</sup>. The controlled phase  $\psi_n$  is to clarify the statistical single photon-based anticorrelation<sup>1-5</sup>, where the anticorrelation on a BS must suffice the magic phase between two input photons:  $\psi_n = \pm(n - 1/2)\pi$  and  $n=1,2,3,\dots$ <sup>6</sup>. Thus, the vagueness in conventional anticorrelation on a BS has been clearly understood and extended into a deterministic feature of nonclassical light generation. Because BS matrix satisfies a  $\pi/2$  phase shift between two split outputs, i.e., reflected and transmitted lights<sup>18</sup>, Fig. 1(a) can be simply represented by a typical MZI as shown in Fig. 1(b)<sup>1</sup>. Due to the preset  $\pi/2$  phase shift on the first BS for  $E_3$  and  $E_4$  in Fig. 1(b), the inserted phase shifter of  $\varphi_n$  must be  $\varphi_n = \pm n\pi$  for the same outputs as in Fig. 1(a)<sup>6</sup>. The intensity correlation  $g^{(2)}$  between two outputs  $I_5$  and  $I_6$  is described by  $g^{(2)} = \frac{\langle I_5 I_6 \rangle}{\langle I_5 \rangle \langle I_6 \rangle}$ , where  $I_j$  is the intensity of  $E_j$ . Thus, conventional MZI becomes a quantum device for nonclassical photon generation with determinacy for a Schrodinger's cat or a NOON state<sup>1,6</sup>.

In the conventional photon bunching phenomenon as shown in a HOM dip or a Bell state using SPDC-based entangled photon pairs, the requirement of  $\psi_n$  in Fig. 1(a) is automatically satisfied by a closed-type  $\chi^{(2)}$ -based three-wave mixing process in a nonlinear medium. In the SPDC nonlinear optical process, however, the choice of the sign of  $\psi_n$  cannot be deterministic due to the bandwidth-wide, probabilistically distributed space-superposed entangled photons as described by, e.g., a polarization entanglement superposition state<sup>2</sup>:  $|\psi\rangle = (|H\rangle_1|V\rangle_2 + e^{i\psi}|V\rangle_1|H\rangle_2)/\sqrt{2}$ . In the case of two independent solid-state emitters, the generated single

photon pair must be phase-locked if excited by the same pump pulse. Thus, the condition of  $\psi_n$  in Fig. 1(a) must be postadjusted to be  $\pm \frac{\pi}{2}$  in the relative phase difference for the anticorrelation or an entangled state generation<sup>3</sup>. The proof of the magic phase of  $\pm \frac{\pi}{2}$  in Fig. 1(a) for nonclassical light generation has already been demonstrated in two independent trapped ions<sup>19</sup>. In Fig. 1(b), the spectral bandwidth ( $\delta\omega$ ) of the input light  $E_0$  should limit the interaction time ( $\tau$ ) or coherence length ( $l_c$ ) in  $g^{(2)}$  anticorrelation. In the application of secured communications<sup>7</sup>, the transmission distance is potentially unlimited, where  $l_c = \frac{c}{\text{mHz}} \sim 10^8$  (km) if sub-mHz linewidth laser is used<sup>20</sup>. In this case, a common phase encoding technique may be advantageous compared to the amplitude modulation technique. According to ref. 21, the maximal indistinguishability induced by perfect quantum superposition represents for maximal coherence, where maximal coherence is a prerequisite for an entangled state or nonclassical light generation.

Figure 1(c) represents a basic building block of the present deterministic control of PBW via coherence optics-based anticorrelation. The output fields in the first building block D of Fig. 1(c), whether it is for  $E_5$  or  $E_6$ , are fed into the block D' by splitting into  $E_7$  and  $E_8$ , resulting in the second-order superposition state. The same phase shifter is used in both D and D' in an asymmetric configuration and simultaneous controls: see the phase shifter  $\Phi(\varphi)$  locates oppositely in each block. If the phase shifter distribution is symmetric, then a unitary transformation is applied for the unconditionally secured classical cryptography<sup>7</sup>. The second-order superposition in Fig. 1(c) offers the fundamental physics of the present coherence-based PBW. The output of the first block D in Fig. 1(c) is described as follows:

$$\begin{bmatrix} E_5 \\ E_6 \end{bmatrix} = [D] \begin{bmatrix} E_0 \\ 0 \end{bmatrix} = \frac{1}{2} \begin{bmatrix} 1 - e^{i\varphi} & i(1 + e^{i\varphi}) \\ i(1 + e^{i\varphi}) & e^{i\varphi} - 1 \end{bmatrix} \begin{bmatrix} E_0 \\ 0 \end{bmatrix}, \quad (1)$$

where  $[D] = [BS][\Phi][BS]$ ,  $[BS] = \frac{1}{\sqrt{2}} \begin{bmatrix} 1 & i \\ i & 1 \end{bmatrix}$ , and  $[\Phi] = \begin{bmatrix} 1 & 0 \\ 0 & e^{i\varphi} \end{bmatrix}$ . As already known in the MZI interferometry, equation (1) shows a  $2\pi$  modulation period in each output intensity:  $I_5 = I_0(1 - \cos(\varphi))$ ;  $I_6 = I_0(1 + \cos(\varphi))$  as shown in Fig. 2(a). Thus, the intensity correlation  $g^{(2)}$  has a  $\pi$  modulation as expected (see the red curve in Fig. 2(a)):

$$g_{\alpha\beta}^{(2)} = [1 - \cos(2\varphi)]/2, \quad (2)$$

where the phase basis for  $g_{\alpha\beta}^{(2)} = 0$  is  $\varphi_n = \pm n\pi$ .

Equation (2) is known as the classical resolution limit or Rayleigh criterion<sup>22</sup>. The output lights,  $E_A$  and  $E_B$ , in the second block D' of Fig. 1(c) are then described by the following relation:

$$\begin{bmatrix} E_A \\ E_B \end{bmatrix} = [D'] [D] \begin{bmatrix} E_0 \\ 0 \end{bmatrix} = -\frac{1}{2} \begin{bmatrix} 1 + e^{i2\varphi} & i(1 - e^{i2\varphi}) \\ -i(1 - e^{i2\varphi}) & 1 + e^{i2\varphi} \end{bmatrix} \begin{bmatrix} E_0 \\ 0 \end{bmatrix}, \quad (3)$$

where  $[D'] = [BS][\Phi'][BS]$  and  $[\Phi'] = \begin{bmatrix} e^{i\varphi} & 0 \\ 0 & 1 \end{bmatrix}$ . Unlike equation (1), equation (2) results in a twice shorter (faster) modulation period (frequency), i.e.,  $\pi/2$  modulation in each intensity of  $I_A$  and  $I_B$ :  $I_A = 2(1 + \cos(2\varphi))$ ;  $I_B = 2(1 - \cos(2\varphi))$  (see Fig. 2(b)). As a result, the intensity correlation  $g^{(2)}$  of  $I_A$  and  $I_B$  in Fig. 1(c) becomes:

$$g_{AB}^{(2)} = [1 - \cos(4\varphi)]/2. \quad (4)$$

Thus, the classical resolution limit of  $\lambda_0/2$  governed by the Rayleigh criterion in Fig. 1(b) is overcome using coherence optics in Fig. 2(b). In equation (4), the phase basis for  $g_{AB}^{(2)} = 0$  is accordingly changed from  $\varphi_n = \pm n\pi$  in Fig. 1(b) to  $\varphi_n = \pm n\pi/2$ . This doubly enhanced resolution of the output intensity in Figs. 1(c) and 2(b) should contradict to the general understating of quantum mechanics because the method of Fig. 1(c) and its result in Fig. 2(b) are perfectly coherent and classical.

Here, it should be noted that such an enhanced phase resolution in Figs. 1(c) and 2(b) has already been well known in a multi-slit experiment in a limited version<sup>22</sup>. Thus, the specific phase relation with  $\varphi_n$  between two superposed coherent lights in MZI of Fig. 1(b) becomes the definite source of nonclassical feature such as

anticorrelation and entanglement<sup>6</sup>. In that sense, the number of superposition state in Fig. 1(c) should be equivalent to the number of entangled photons in conventional quantum PBW (see equations (2) and (4)). Therefore, the asymmetrically coupled MZI scheme composed of D and D' in Fig. 1(c) represents the basic unit of the present coherence version of PBW. Then, the higher-order coherence PBW can also be achieved by simply connecting the asymmetrical unit of Fig. 1(c) in a series (discussed in Fig. 3).

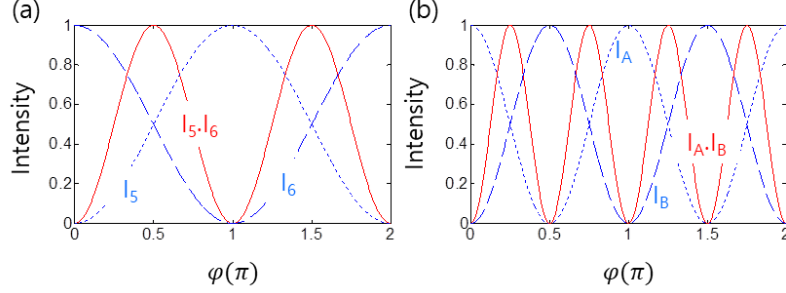


Fig. 2. Numerical calculations for  $g^{(2)}$  intensity correlation of Fig. 1(c). (a) Red:  $I_5 I_6$  (normalized), Dotted:  $I_5$ , Dashed:  $I_6$ . (b) Red:  $I_A I_B$  (normalized), Dotted:  $I_A$ , Dashed:  $I_B$ . The input field intensity of  $E_0 = 1$  is assumed.

Figure 2 shows numerical calculations for Fig. 1(c) to support the present theory of the deterministic control of PBW in a coherence regime. Figure 2(a) shows a typical MZI result of Fig. 1(b) by solving equation (1), where each output intensity represents the classical limit. As expected, the conventional MZI scheme gives a spectroscopic resolution of  $\lambda_0/2$ , which is the Rayleigh limit in classical physics. This classical resolution limit is now understood as the first order of the present deterministic control of PBW:  $\lambda_{CB} = \lambda_0/2\zeta$ , where  $\zeta$  is the number of MZI block (or superposition state in the form of Fig. 1(b)), and  $\lambda_{CB}$  indicates the present coherence PBW. Here, it should be noted that each MZI block in Fig. 1(b) is equivalent to  $N=2$  in quantum PBW for an entanglement superposition description at  $|\psi\rangle = (|N\rangle_A |0\rangle_B + |0\rangle_A |N\rangle_B)/\sqrt{2}$ :  $2\zeta = N$ . In other words, a typical MZI is a quantum device for anticorrelation or nonclassical light generation if  $\varphi_n = \pm n\pi$  is satisfied. The intensity correlation of  $g_{AB}^{(2)}$  in equation (4) is numerically calculated in Fig. 2(b): see red curve. The demonstration of  $\lambda_{CB} = \lambda_0/4$  in Fig. 2(b) proves the present theory of coherence PBW based on Fig. 1(c). Thus, it is concluded that the present coherence PBW in Fig. 1(c) is equivalent to the quantum PBW based on entangled photons with an additional benefit of deterministic controllability.

For the higher order  $\lambda_{CB}$ , the basic scheme of Fig. 1(c) needs to be repeated in a series or circulated in a feedback form as shown in Fig. 3(a). In this circulation configuration, the  $\eta$  stands for reflectance on the end mirrors. Defining  $[CM] = [D'][D]$ , the  $n^{\text{th}}$  order output fields in Fig. 3(a) can be obtained from equation (3) (see Appendix):

$$\begin{bmatrix} E_A \\ E_B \end{bmatrix}^n = [CM]^n \eta^{2n} \begin{bmatrix} E_0 \\ 0 \end{bmatrix}, \quad (5-1)$$

$$= \frac{1}{2} (-1)^n \eta^{2n} \begin{bmatrix} (1 + e^{i2n\varphi}) & i(1 - e^{i2n\varphi}) \\ -i(1 - e^{i2n\varphi}) & (1 + e^{i2n\varphi}) \end{bmatrix} \begin{bmatrix} E_0 \\ 0 \end{bmatrix}, \quad (5-2)$$

$$(E_A)^n = \frac{E_0}{2} (-1)^n \eta^{2n} (1 + e^{i2n\varphi}), \quad (5-3)$$

$$(E_B)^n = i \frac{E_0}{2} (-1)^{n+1} \eta^{2n} (1 - e^{i2n\varphi}), \quad (5-4)$$

From equations (5-3) and (5-4) the related  $n^{\text{th}}$  order intensities are obtained assuming each  $n^{\text{th}}$  order can be extracted (actual cavity output is discussed below):

$$(I_A)^n = \frac{1}{2}\eta^{4n}I_0[1 + \cos(2n\varphi)], \quad (6-1)$$

$$(I_B)^n = \frac{1}{2}\eta^{4n}I_0[1 - \cos(2n\varphi)]. \quad (6-2)$$

where  $I_0 = E_0 E_0^*$ . For the actual intensity output, it must be multiplied by  $(1 - \eta)$ . However, this  $\eta$ -related prefactor in equations (6-1) and (6-2) is not important because  $E_0$  in Fig. 3(a) is coherent light whose input intensity  $I_0$  has no limit. As a result, the  $n^{\text{th}}$  order intensity correlation  $g_n^{(2)}$  becomes:

$$g_n^{(2)} = \frac{\langle (I_A)^n (I_B)^n \rangle}{\langle (I_A)^n \rangle \langle (I_B)^n \rangle} = \frac{1}{2}[1 - \cos(4n\varphi)]. \quad (7)$$

Thus, the general equation for the coherence PBW in the  $n^{\text{th}}$  order is described by:

$$\lambda_{CB}^{(n)} = \lambda_0/4n, \quad (8)$$

where  $n$  is the number of repetition. For  $n=1$ , there are basic building blocks of D and D' equivalent to the four-photon ( $N=4$ ) case in quantum PBW<sup>11-14</sup>. Because equation (8) is deterministic, the present coherence PBW is powerful compared with conventional quantum counterpart in terms of  $N$  number. This fact may open a door to coherence-quantum metrology based on on-demand  $\lambda_{CB}^{(n)}$ . For the impracticality of quantum PBW, it takes  $\sim 2$  hour acquisition time just for  $N=18$ <sup>14</sup>.

Figure 3(a) represents a general scheme of the higher-order coherence PBW in a repeated (or circulated) configuration as analyzed above. To minimize the light intensity loss in the circulation process, the end mirrors are kept to be highly reflective, resulting in an optical cavity. As analyzed in equations (5) and (8), the number of repetition is denoted by  $n$ , where each cycle is equivalent to two MZI blocks or the four-photon in quantum PBW:  $\lambda_B (= \frac{\lambda_0}{4})$ . Figure 3(b) shows numerical calculations using equations (6-1) and (6-2) for the case of  $n^{\text{th}}$  order intensity correlation  $g_n^{(2)}$ . As demonstrated, the coherent  $\lambda_{CB}^{(n)}$  is clearly equivalent to the quantum  $\lambda_B$ . Compared with impractically long acquisition time in quantum PBW<sup>12-14</sup>, the higher order  $\lambda_{CB}^{(n)}$  is deterministic in real time. The higher order  $n$  in Fig. 3(b) is only limited by  $\eta$ . Each  $n^{\text{th}}$  order intensity modulation period is twice longer than  $g_n^{(2)}$  obtained in Fig. 3(b) as shown in equations (6-1) and (6-2). For commercially available end mirrors whose  $\eta = 0.999$ , the repetition of  $n=10^3$  is possible, where the phase resolution enhancement in intensity output  $I_A$  and  $I_B$  is  $10^3$ , too.

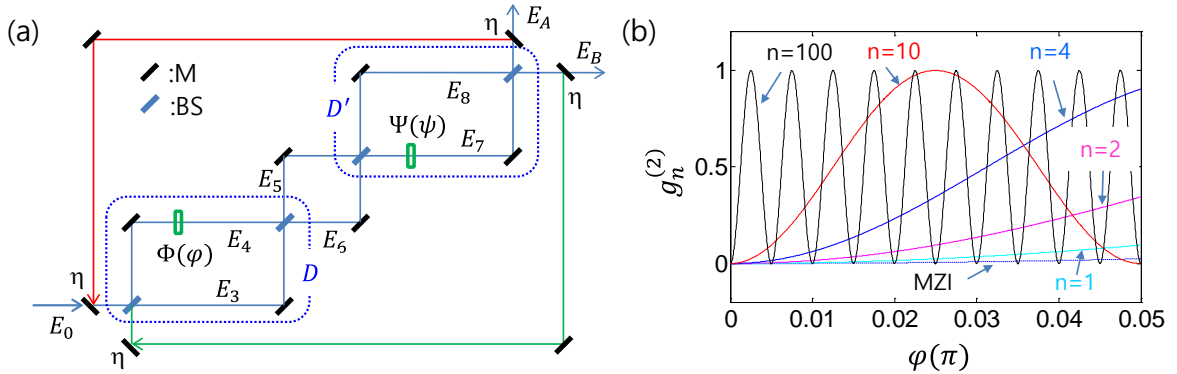


Fig. 3. A photonic de Broglie wavelength generator. (a) A feedback scheme of PBW.  $\eta$  is reflectance for the recursive lights. (b) Numerical calculations for (a), where  $n$  indicates the number of repetition. MZI represents a reference of a classical limit whose period is  $\pi$  as shown in Fig. 2(a).

In Fig. 3(a), however, all  $n$  ordered fields should interfere one another before coming out of the cavity resulting in multi-wave interference. This interference does not deteriorate the resolution enhancement shown in Fig. 3(b). For  $\varphi_{mn} = \pm \left(\frac{m}{n}\right)\pi$ ,  $(E_A)^n = (-1)^n \eta^{2n} E_0$  and  $E_B = 0$ , where  $E_A = \sum_{n=1}^N (E_A)^n = -E_0(1 - \eta^2)(1 + \eta^4 + \eta^8 + \eta^{12} + \dots)$ . For  $\varphi_{mn} = \pm \left(\frac{(2m+1)}{2n}\right)\pi$ , however,  $(E_A)^n = 0$  and  $E_B = i(-1)^{n+1} \eta^{2n} E_0$ ,

where  $E_B = \sum_{n=1}^N (E_B)^n = -iE_0(1 - \eta^2)(1 + \eta^4 + \eta^8 + \eta^{12} + \dots)$ . Thus, the output intensities  $I_A$  and  $I_B$  become zero at  $\varphi_{mn} = \pm \left(\frac{m}{n}\right)\pi$  and  $\varphi_{mn} = \pm \left(\frac{(2m+1)}{2n}\right)\pi$ , respectively, if  $\eta \sim 1$ . In the ordered amplitudes, however, there is a sign flip between  $n^{\text{th}}$  and  $(n+1)^{\text{th}}$  due to the prefactor of  $(-1)^n$  or  $(-1)^{n+1}$ . Thus, if the phase  $\varphi_{mn}$  is chosen to be  $m=n$ , e.g.,  $\varphi_{nn} = \pm\pi$  for  $(E_A)^n$ , there is no sign flip for all  $(E_A)^n$ . This phase of  $\varphi_{nn}$  represents a co-phase for all  $n$ . Thus,  $E_A$  results in a constructive interference:  $E_{A(m=n)} = E_0(\eta + \eta^3 + \eta^5 + \eta^7 + \eta^9 + \eta^{11} + \eta^{13} + \dots)$ . For the case of very high Finesse ( $\eta \sim 1$ ), thus,  $E_A \sim NE_0$ , where the maximum  $n$  ( $N$ ) is determined by the Finesse. This result is exactly same as the many-slit diffraction case of Young's many-slit experiments<sup>22</sup>, where  $I_A = N^2 I_0$  for  $\eta = 1$ . In an actual case, however,  $I_A$  decreases as  $n$  ( $m$ ) increases in both cases. In other words, the cavity Finesse in Fig. 3(a) plays a role of the slit bandwidth as well as the slit number  $N$ . In the many-slit diffraction, each slit width confines the  $N^2$  intensity according to the Rayleigh criterion<sup>22</sup>.

In conclusion, the deterministic control of photonic de Broglie waves (PBW) was presented in a purely coherence manner for both fundamental physics and potential applications of coherence-quantum metrology using an asymmetrically configured double MZI scheme. For this, the output from the asymmetrically configured double MZI scheme was circulated for higher-order coherence PBW. The analytical expression and its numerical calculations showed an equivalent feature to the quantum PBW, where number of MZIs in the present coherence PBW is equivalent to the entangled photon number  $N$  in quantum PBW. The random phase noise of the MZI system caused by mechanical vibrations, air turbulence, and temperature variations at  $\leq$  MHz rate may be eliminated by either taking potentially the same beam path for the MZI configuration such as in Sagnac interferometer or controlling the environmental phase noise down to a sub-mHz range with the state-of-the-art laser stabilization technique<sup>23</sup>. As a result, present coherence PBW can be directly applied to high precision optical spectroscopy or quantum metrology such as optical clock<sup>24</sup>, gravitational wave detection<sup>25</sup>, quantum lithography<sup>15,16</sup>, and quantum sensors<sup>17</sup>. The seemingly contradiction of coherence PBW to quantum physics is reconciled by quantum superposition of MZI paths, where MZI is treated as a quantum device like BS if the magic phase is involved<sup>1,6</sup>. The present scheme of Fig. 3(a) may open a door to coherence-quantum metrology for deterministic control of photonic de Broglie wavelength at higher orders in real time and for on-demand. Eventually, the present asymmetric double MZI-based photonic de Broglie wave generation scheme may apply for non-classical light generation such as deterministic entangled photons and photonic qubits, resulting in on-demand quantum information processing (discussed elsewhere).

## [Appendix]

$$\begin{aligned} \begin{bmatrix} E_A \\ E_B \end{bmatrix}^1 &= [CM]^1 \begin{bmatrix} E_0 \\ 0 \end{bmatrix}, \\ &= (-1)^1 \left(\frac{1}{2}\right)^1 \eta^0 \begin{bmatrix} 1 + e^{i2\varphi} & i(1 - e^{i2\varphi}) \\ -i(1 - e^{i2\varphi}) & 1 + e^{i2\varphi} \end{bmatrix} \begin{bmatrix} E_0 \\ 0 \end{bmatrix}. \end{aligned}$$

For  $\varphi = \pm m\pi$ ,  $E_A = -\eta E_0$  and  $E_B = 0$ . Here,  $m=0,1,2,3\dots$

For  $\varphi = \pm \frac{(2m+1)}{2}\pi$ ,  $E_A = 0$  and  $E_B = i\eta E_0$ .

$$\begin{aligned} \begin{bmatrix} E_A \\ E_B \end{bmatrix}^2 &= [CM]^2 \begin{bmatrix} E_0 \\ 0 \end{bmatrix}, \\ &= [CM][CM]\eta^2 \begin{bmatrix} E_0 \\ 0 \end{bmatrix}, \\ &= (-1)^2 \left(\frac{1}{2}\right)^2 \eta^2 \begin{bmatrix} 1 + e^{i2\varphi} & i(1 - e^{i2\varphi}) \\ -i(1 - e^{i2\varphi}) & 1 + e^{i2\varphi} \end{bmatrix} \begin{bmatrix} 1 + e^{i2\varphi} & i(1 - e^{i2\varphi}) \\ -i(1 - e^{i2\varphi}) & 1 + e^{i2\varphi} \end{bmatrix} \begin{bmatrix} E_0 \\ 0 \end{bmatrix}, \\ &= (-1)^2 \left(\frac{1}{2}\right)^2 \eta^2 \begin{bmatrix} (1 + e^{i2\varphi})^2 + (1 - e^{i2\varphi})^2 & 2i(1 + e^{i2\varphi})(1 - e^{i2\varphi}) \\ -2i(1 + e^{i2\varphi})(1 - e^{i2\varphi}) & (1 + e^{i2\varphi})^2 + (1 - e^{i2\varphi})^2 \end{bmatrix} \begin{bmatrix} E_0 \\ 0 \end{bmatrix}, \\ &= \frac{1}{2}(-1)^2 \eta^2 \begin{bmatrix} (1 + e^{i4\varphi}) & i(1 - e^{i4\varphi}) \\ -i(1 - e^{i4\varphi}) & (1 + e^{i4\varphi}) \end{bmatrix} \begin{bmatrix} E_0 \\ 0 \end{bmatrix}. \end{aligned}$$

For  $\varphi = \pm m\pi/2$ ,  $(E_A)^{n=2} = \eta^2 E_0$  and  $E_B = 0$ .

For  $\varphi = \pm \frac{(2m+1)}{4}\pi$ ,  $(E_A)^{n=2} = 0$  and  $E_B = -i\eta^2 E_0$ .

$$\begin{aligned} \begin{bmatrix} E_A \\ E_B \end{bmatrix}^3 &= [CM]^3 \begin{bmatrix} E_0 \\ 0 \end{bmatrix}, \\ &= [CM][CM][CM]\eta^4 \begin{bmatrix} E_0 \\ 0 \end{bmatrix}, \\ &= (-1)^3 \left(\frac{1}{2}\right)^3 2^1 \eta^4 \begin{bmatrix} (1 + e^{i2\varphi}) & i(1 - e^{i2\varphi}) \\ -i(1 - e^{i2\varphi}) & (1 + e^{i2\varphi}) \end{bmatrix} \begin{bmatrix} (1 + e^{i4\varphi}) & i(1 - e^{i4\varphi}) \\ -i(1 - e^{i4\varphi}) & (1 + e^{i4\varphi}) \end{bmatrix} \begin{bmatrix} E_0 \\ 0 \end{bmatrix}, \\ &= \frac{1}{2}(-1)^3 \eta^4 \begin{bmatrix} (1 + e^{i6\varphi}) & i(1 - e^{i6\varphi}) \\ -i(1 - e^{i6\varphi}) & (1 + e^{i6\varphi}) \end{bmatrix} \begin{bmatrix} E_0 \\ 0 \end{bmatrix}. \end{aligned}$$

For  $\varphi = \pm m\pi/3$ ,  $(E_A)^{n=2} = -\eta^4 E_0$  and  $E_B = 0$ .

For  $\varphi = \pm \frac{(2m+1)}{6}\pi$ ,  $(E_A)^{n=2} = 0$  and  $E_B = i\eta^4 E_0$ .

$$\begin{aligned} \begin{bmatrix} E_A \\ E_B \end{bmatrix}^4 &= [CM]^4 \eta^6 \begin{bmatrix} E_0 \\ 0 \end{bmatrix}, \\ &= (-1)^4 \left(\frac{1}{2}\right)^4 2^2 \eta^6 \begin{bmatrix} (1 + e^{i2\varphi}) & i(1 - e^{i2\varphi}) \\ -i(1 - e^{i2\varphi}) & (1 + e^{i2\varphi}) \end{bmatrix} 2^2 \begin{bmatrix} (1 + e^{i6\varphi}) & i(1 - e^{i6\varphi}) \\ -i(1 - e^{i6\varphi}) & (1 + e^{i6\varphi}) \end{bmatrix} \begin{bmatrix} E_0 \\ 0 \end{bmatrix}, \\ &= \frac{1}{2}(-1)^4 \eta^6 \begin{bmatrix} (1 + e^{i8\varphi}) & i(1 - e^{i8\varphi}) \\ -i(1 - e^{i8\varphi}) & (1 + e^{i8\varphi}) \end{bmatrix} \begin{bmatrix} E_0 \\ 0 \end{bmatrix}. \end{aligned}$$

For  $\varphi = \pm m\pi/4$ ,  $(E_A)^{n=2} = \eta^6 E_0$  and  $E_B = 0$ .

For  $\varphi = \pm \frac{(2m+1)}{8}\pi$ ,  $(E_A)^{n=2} = 0$  and  $E_B = -i\eta^6 E_0$ .

From the above relations, the following  $n^{\text{th}}$  order outputs can be driven:

$$\begin{aligned} \begin{bmatrix} E_A \\ E_B \end{bmatrix}^n &= [CM]^n \eta^{2n} \begin{bmatrix} E_0 \\ 0 \end{bmatrix}, \\ &= \frac{1}{2}(-1)^n \eta^{2n} \begin{bmatrix} (1 + e^{i2n\varphi}) & i(1 - e^{i2n\varphi}) \\ -i(1 - e^{i2n\varphi}) & (1 + e^{i2n\varphi}) \end{bmatrix} \begin{bmatrix} E_0 \\ 0 \end{bmatrix}. \end{aligned}$$

For  $\varphi = \pm \left(\frac{m}{n}\right)\pi$ ,  $(E_A)^n = (-1)^n \eta^{2n} E_0$  and  $E_B = 0$ .

For  $\varphi = \pm \left(\frac{(2m+1)}{2n}\right)\pi$ ,  $(E_A)^n = 0$  and  $E_B = i(-1)^{n+1} \eta^{2n} E_0$ .

As a result,  $(I_A)^n (I_B)^n = \eta^{4n} I_0$ , where  $I_0 = E_0 E_0^*$ .

Owing to the cavity effect in Fig. 3(a), however, all the  $n$  ordered fields interfere one another resulting in the following:

$$\begin{aligned} E_A &= \sum_{n=1}^N (E_A)^n, \\ &= E_0 \sum_{n=1}^N (-1)^n \eta^{2n}, \\ &= E_0 (1 - \eta^2 + \eta^4 - \eta^6 + \eta^8 - \eta^{10} + \dots), \\ &= E_0 [(1 + \eta^4 + \eta^8 + \dots) - (\eta^2 + \eta^6 + \eta^{10} + \dots)], \\ &= -E_0 (1 - \eta^2)(1 + \eta^4 + \eta^8 + \eta^{12} + \dots). \end{aligned}$$

$$\begin{aligned} E_B &= \sum_{n=1}^N (E_B)^n, \\ &= iE_0 (-1)^{n+1} \eta^{2n}, \\ &= -iE_0 (1 - \eta^2 + \eta^4 - \eta^6 + \eta^8 - \eta^{10} + \eta^{12} + \dots), \\ &= -iE_0 (1 - \eta^2)(1 + \eta^4 + \eta^8 + \eta^{12} + \dots). \end{aligned}$$

Therefore, the output intensity in Fig. 3(a) is as follows:

$$\begin{aligned} I_A &= E_A E_A^*, \\ &= I_0 (1 - \eta^2)^2 (1 + \eta^4 + \eta^8 + \eta^{12} + \dots)^2 \sim 0. \\ I_B &= E_B E_B^* = I_A. \end{aligned}$$

Thus, the output intensity  $I_A$  becomes zero at  $\varphi_{mn} = \pm \left(\frac{m}{n}\right)\pi$  if  $\eta \sim 1$  for a high Finesse cavity. So does  $I_B$  at  $\varphi = \pm \left(\frac{(2m+1)}{2n}\right)\pi$ .

## Reference

1. Grangier, P., Roger, G. & Aspect, A. Experimental evidence for a photon anticorrelation effect on a beam splitter: A new light on single-photon interference. *Europhys. Lett.* **1**, 173-179 (1986).
2. Hong, C. K., Ou, Z. Y. & Mandel, L. Measurement of subpicosecond time intervals between two photons by interference. *Phys. Rev. Lett.* **59**, 2044-2046 (1987).
3. Lettow, R. *et al.*, Quantum interference of tunably indistinguishable photons from remote organic molecules. *Phys. Rev. Lett.* **104**, 123605 (2010).
4. Peruzzo, A., Shadbolt, P., Brunner, N., Popescu, S. & O'Brien, J. L. A quantum delayed-choice experiment. *Science* **338**, 634-637 (2012).
5. Deng, Y.-H. *et al.*, Quantum interference between light sources separated by 150 million kilometers. *Phys. Rev. Lett.* **123**, 080401 (2019).
6. Ham, B. S. The origin of anticorrelation for photon bunching on a beam splitter. arXiv:1911.07174v2 (2019).
7. Ham, B. S. Unconditionally secured classical cryptography using quantum superposition and unitary transformation. arXiv:1807.04233 (2019).
8. Bohr, N. The quantum postulate and the recent development of atomic theory. *Nature* **121**, 580-590 (1928).
9. Wootters, W. K. & Zurek, W. H. Complementarity in the double-slit experiment: Quantum nondeparability and quantitative statement of Bohr's principle. *Phys. Rev. D* **19**, 473-484 (1979).
10. Greenberger, D. M. Horne, M. A. & Zeilinger, A. Multiparticle interferometry and the superposition principle. *Phys. Today* **46**(8), 22-29 (1993).
11. Jacobson, J., Gjörk, G., Chung, I. & Yamamoto, Y. Photonic de Broglie waves. *Phys. Rev. Lett.* **74**, 4835-4838 (1995).
12. Edamatsu, K., Shimizu, R. & Itoh, T. Measurement of the photonic de Broglie wavelength of entangled photon pairs generated by parametric down-conversion. *Phys. Rev. Lett.* **89**, 213601 (2002).
13. Walther, P., Pan, J.-W., Aspelmeyer, M., Ursin, R., Gasparon, S. & Zeilinger, A. De Broglie wavelength of a non-local four-photon state. *Nature* **429**, 158-161 (2004).
14. Wang, X.-L. *et al.*, 18-qubit entanglement with six photons' three degree of freedom. *Phys. Rev. Lett.* **120**, 260502 (2018).
15. Kok, P., Braunstein, S. L. & Dowling, J. P. Quantum lithography, entanglement, and Heisenberg-limited parameter estimation. *J. Opt. B: Quantum Semiclass. Opt.* **6**, S811-S815 (2004).
16. Clerk, A. A. *et al.*, Introduction to quantum noise, measurement, and amplification. *Rev. Mod. Phys.* **82**, 1155-1208 (2010).
17. Pezze, L. *et al.*, Quantum metrology with nonclassical states of atomic ensemble. *Rev. Mod. Phys.* **90**, 035005 (2018).
18. Degiorgio, V. Phase shift between the transmitted and the reflected optical fields of a semireflecting lossless mirror is  $\pi/2$ . *Am. J. Phys.* **48**, 81-82 (1980).
19. Solano, E., de Matos Filho, R. L. & Zagury, N. Deterministic Bell states and measurement of the motional state of two trapped ions. *Phys. Rev. A* **59**, R2539-R2543 (1999).
20. Kessler, T. *et al.* A sub-40-mHz-linewidth laser based on a silicon single-crystal optical cavity. *Nature Photon.* **6**, 687-692 (2012).
21. Mandel, L. Coherence and indistinguishability. *Opt. Lett.* **16**, 1882-1883 (1991).
22. Pedrotti, F. L., Pedrotti, L. M. & Pedrotti, L. S. *Introduction to Optics*, 3<sup>rd</sup> Ed., Ch.11 (Pearson Addison Wesley) (2007).
23. Salomon, Ch., Hils, D. & Hall, J. L. Laser stabilization at the millihertz level. *J. Opt. Soc. Am. B* **5**, 1576-1587 (1988).
24. Ludlow, A. D., Boyd, M. M., Ye, J., Peik, E. & Schmidt, P. O. Optical atomic clock. *Rev. Mod. Phys.* **87**, 637-701 (2015).
25. Grote, H., Danzmann, K., Dooley, K. L., Schnabel, R., Slutsky, J. & Vahlbruch, H. First Long-Term Application of Squeezed States of Light in a Gravitational-Wave Observatory. *Phys. Rev. Lett.* **110**, 181101 (2013).